Supporting Information for

Functional calcium-responsive parathyroid glands generated using single-step blastocyst complementation

Mayuko Kano[1,2,3], Naoaki Mizuno[1,2], Hideyuki Sato[1,2], Takaharu Kimura[4], Rei Hirochika[4], Yasumasa Iwasaki[5,6], Naoko Inoshita[7], Hisato Nagano[1,2,8], Mariko Kasai[1,2], Hiromi Yamamoto[1,2], Tomoyuki Yamaguchi[2,9], Hidetaka Suga[10], Hideki Masaki[1,2], *Eiji Mizutani[1,2,4,], and *Hiromitsu Nakauchi[1,2,11]

[1]Stem Cell Therapy Laboratory, Advanced Research Institute, Tokyo Medical and Dental University (TMDU), 1-5-45 Yushima, Bunkyo-Ku, Tokyo 113-8510, Japan

[2]Division of Stem Cell Therapy, Center for Stem Cell Biology and Regenerative Medicine, Institute of Medical Science, University of Tokyo, 4-6-1 Shirokanedai, Minato-ku, Tokyo 108-8639, Japan

[3]Metabolism and Endocrinology, Department of Medicine, St. Marianna University School of Medicine, 2-16-1 Sugao, Miyamae-ku, Kawasaki, Kanagawa 216-8511, Japan

[4]Laboratory of Stem Cell Therapy, Institute of Medicine, University of Tsukuba, 1-1-1 Tennodai, Tsukuba 305-8577, Japan

[5]Department of Clinical Nutrition, Faculty of Health Science, Suzuka University of Medical Science, 1001-1 Kishioka-cho, Suzuka, Mie 510-0293, Japan

[6]Department of Endocrinology, Metabolism, and Nephrology, Kochi Medical School, Kochi University, 185-1 Kohasu, Oko-cho, Nankoku, Kochi 783-8505, Japan

[7] Department of Pathology, Moriyama Memorial Hospital, 4-3-1 Kitakasai, Edogawa-ku, Tokyo 134-0081, Japan

[8]Department of Plastic and Reconstructive Surgery, National Defense Medical College, 3–2

Namiki, Tokorozawa, Saitama 359-8513, Japan

[9]Laboratory of Regenerative Medicine, Tokyo University of Pharmacy and Life Science, 1432-1 Horinouchi, Hachioji, Tokyo 192-0392, Japan

[10]Department of Endocrinology and Diabetes, Nagoya University Graduate School of Medicine, 65 Tsurumai-cho, Showa-ku, Nagoya 466-8550, Japan

[11]Institute for Stem Cell Biology and Regenerative Medicine, Stanford University School of Medicine, Sanford, CA 94305, USA

***To whom correspondence should be addressed**

Hiromitsu Nakauchi, M.D., Ph.D.
Institute for Stem Cell Biology and Regenerative Medicine
Stanford University School of Medicine, Sanford, CA 94305, USA
Tel: +1-650-497-4365
Fax: +1-650-497-5794
E-mail: nakauchi@stanford.edu

Eiji Mizutani, Ph.D.
Laboratory of Stem Cell Therapy, Institute of Medicine
University of Tsukuba, 1-1-1 Tennodai, Tsukuba 305-8577, Japan.
Tel: +81-29-853-3287,
Fax: +81-29-853-3115
E-mail: emizutani@md.tsukuba.ac.jp

This PDF file includes:
Figures S1 to S6
Tables S1 to S3

Supplementary Figure Legends

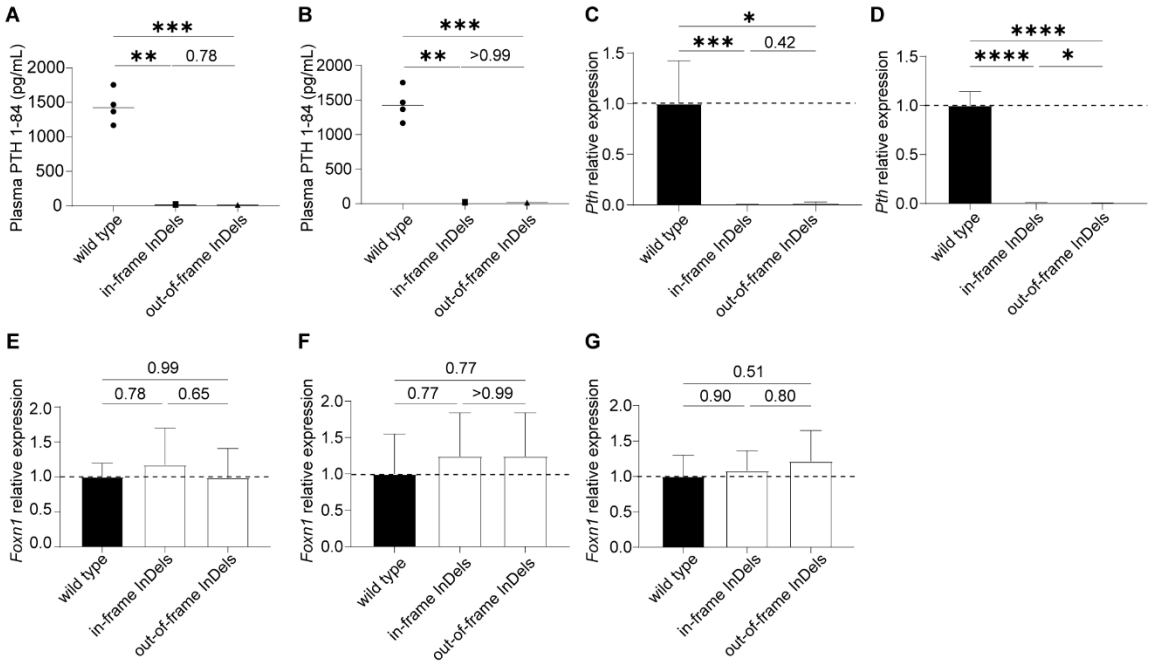

Supplementary Figure 1 (S1). Phenotypes of *Gcm2* KO mice on different genetic backgrounds.

(A) Plasma PTH levels in wild type and *Gcm2* mutant mice on C57BL/6N (B6) background. Wild type, n=5. *Gcm2* mutants with in-frame InDels, n=6. *Gcm2* mutants with out-of-frame InDels, n=6. **(B)** Plasma PTH levels in wild type and *Gcm2* mutant mice on B6 × DBA/2 (BDF1) background**.** Wild type, n=10. *Gcm2* mutants with in-frame InDels, n=12. *Gcm2* mutants with out-of-frame InDels, n=5. **(C)** *Pth* mRNA expression in wild type and *Gcm2* mutant mice on the B6 background. Wild type, n=5. *Gcm2* mutants with in-frame InDels, n=6. *Gcm2* mutants with out-of-frame InDels, n=12. **(D)** *Pth* mRNA expression in wild type and *Gcm2* mutant mice on BDF1 background. Wild type, n=7. *Gcm2* mutants with in-frame InDels, n=5. *Gcm2* mutants with out-of-frame InDels, n=6. (**E**) *Foxn1* mRNA expression in wild type and *Gcm2* mutant mice on B6 background. Wild type, n=5. *Gcm2* mutants with in-frame InDels, n=6. *Gcm2* mutants with out-of-frame InDels, n=12. (**F**) *Foxn1* mRNA expression in wild type and *Gcm2* mutant mice on B6D2F1 × B6 (BDF1B6) background. Wild type, n=6. *Gcm2* mutants with in-frame InDels, n=5. *Gcm2* mutants with out-of-frame InDels, n=5. (**G**) *Foxn1* mRNA expression in wild type and *Gcm2*-mutant mice on BDF1 background. Wild type, n=8. *Gcm2* mutants with in-frame InDels, n=5. *Gcm2* mutants with out-of-frame InDels, n=5. (**C**–**G**) Graphed

values, mean with s.d. * $P \leq 0.05$, ** $P \leq 0.01$, *** $P \leq 0.001$, **** $P \leq 0.0001$ using one sample t-test and Mann Whitney test with Bonferroni's correction (**A**), Brown-Forsythe ANOVA test with Dunnett's T3 multiple comparisons test (**B**, **D**), Kruskal-Wallis test with Dunn's multiple comparisons test (**C**), one-way ANOVA test with Tukey's multiple comparisons test (**E**–**G**).

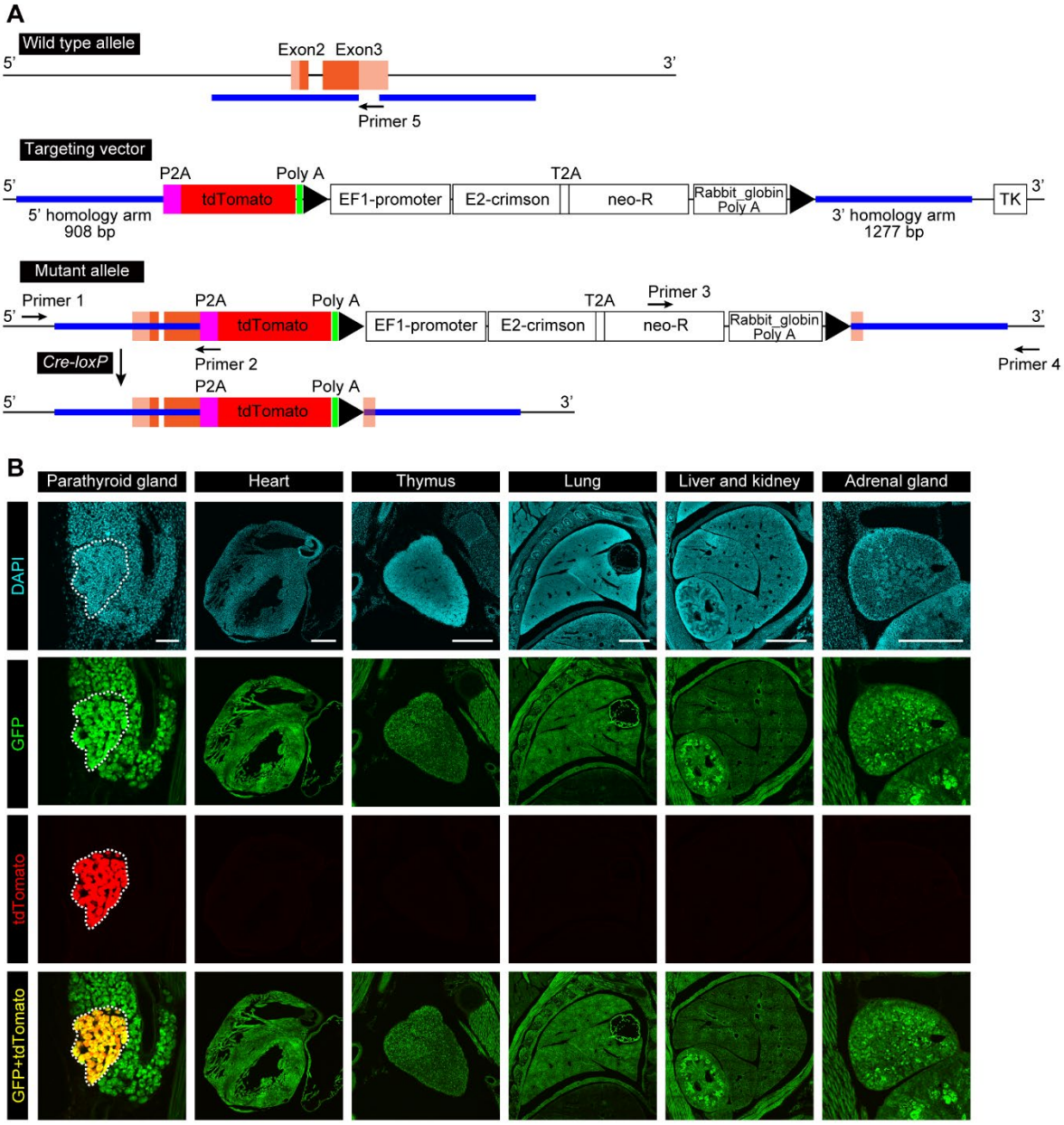

Supplementary Figure 2 (S2). Characteristics of chimeric mice derived from Pth-tdTomato mESCs.

(**A**) Generation of tdTomato – knock-in mESCs at *Pth* locus (C57BL/6N-*Tg(CAG-EGFP)Pth*$^{tm1(P2A\text{-}tdTomato)}$ES1). Targeting vector construction and targeting strategy.

(**B**) Immunostaining of various organs in chimeric mice with high chimerism (> 99%). Note absence of tdTomato expression outside PTGs.

DAPI (cyan), GFP (green), tdTomato (red). Scale bars: 100 μm (PTG), 500 μm (heart,

thymus, and adrenal gland), 1 mm (lung, liver, and kidney).

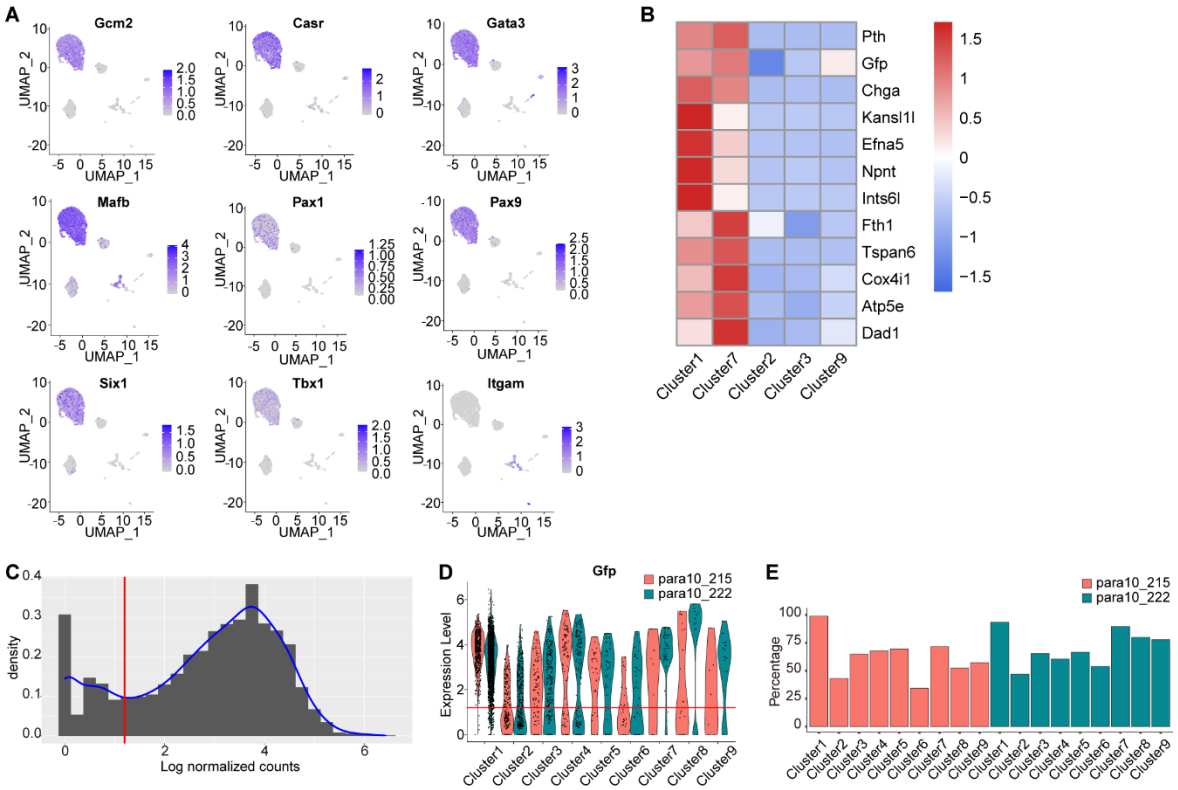

Supplementary Figure 3 (S3). Single-cell RNA-seq findings of mESC-derived PTGs. (**A**) Feature plots on the UMAP showing *Gcm2*, *Casr*, *GATA-binding protein 3* (*Gata3*), *v-maf musculoaponeurotic fibrosarcoma oncogene homolog B* (*MafB*), *Paired box 1* (*Pax1*), *Pax9*, *Sine oculis homeobox 1* (*Six1)*, *T-box transcription factor 1* (*Tbx1*), and *integrin alpha M* (*Itgam*) gene expression. (**B**) Heatmap based on cluster markers. (**C**) Histogram based on normalized *Gfp* count data, all cells. Blue, density curve. Red, threshold between *Gfp*-high and *Gfp*-low (|cutoff for *Gfp* expression). (**D**) Violin plots displaying *Gfp* expression for each experiment. Red line, threshold as in (C). (**E**) Percentage, based on threshold, of *Gfp* expression for each experiment.

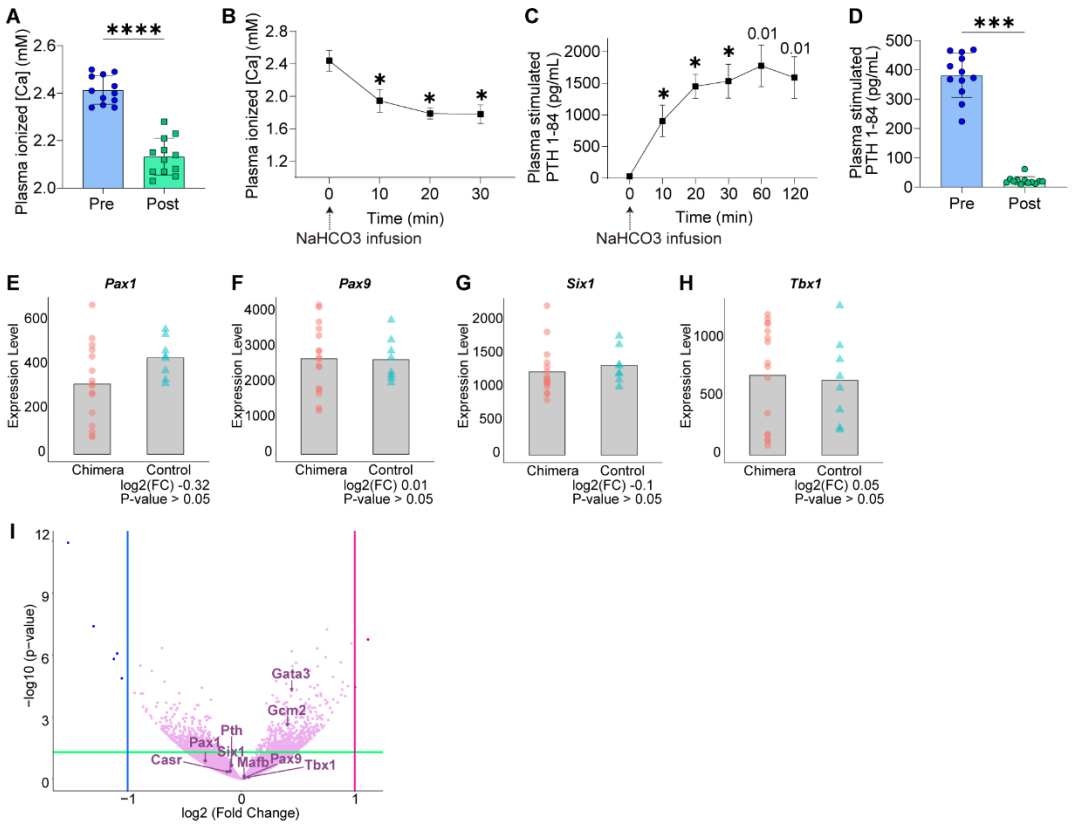

Supplementary Figure 4 (S4). Characterization of mESC-derived PTGs.

(**A**) Plasma [Ca] pre- and post-parathyroidectomy in C57BL/6-*Pth*$^{tm1(P2A\text{-}tdTomato)}$ mice. n=12. (**B, C**) Changes in plasma ionized [Ca] (**B**) and PTH 1-84 (**C**) upon sodium bicarbonate infusion test in wild type B6 mice. All points, n=5 (**B**). 0 min, n=6. 10min, n=6. 20 min, n=3. 30 min, n=6. 60 min, n=3. 120 min, n=3 (**C**). (**D**) Plasma stimulated PTH 1-84 levels pre- and post-parathyroidectomy in C57BL/6-*Pth*$^{tm1(P2A\text{-}tdTomato)}$ mice. n=12. Same samples as (A). (**E**–**H**) Bulk RNA-seq data of PTG cells. Differentially expressed genes (DEG) analysis using DESeq2. log2(FC) means fold changes of chimera gene counts against control (C57BL/6-*Pth*$^{tm1(P2A\text{-}tdTomato)/+}$ mouse). (**I**) Volcano plot from log2(FC) and p-value. DEGs are highlighted as red or blue dots (|log2FC| >1, *p*-value < 0.05).

* $P \leq 0.05$, *** $P \leq 0.001$, **** $P \leq 0.0001$ using Wilcoxon test (**A**), paired t-tests with Bonferroni's correction (**B**, **C**), and paired t-test (**D**).

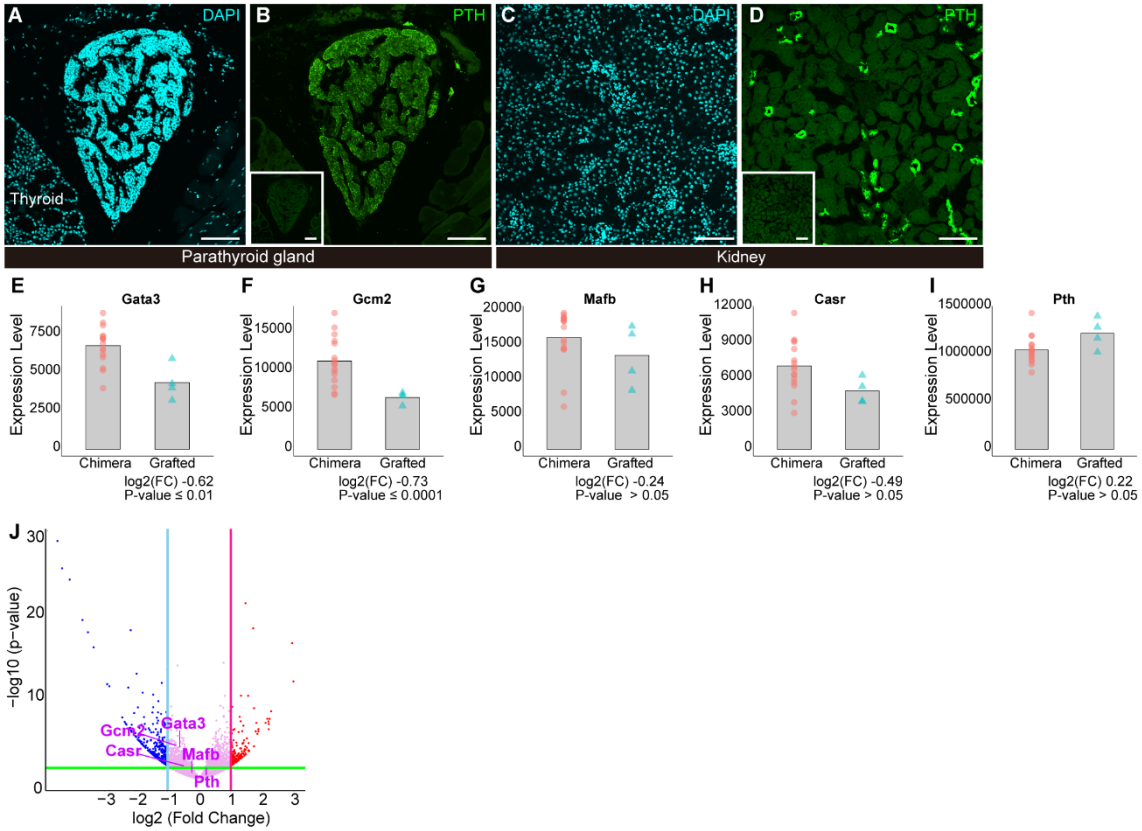

Supplementary Figure 5 (S5). Immunohistochemical and bulk RNA-seq findings in grafted mESC-derived PTGs.

(**A**–**D**) Parathyroid gland and kidney of wild type B6 mouse stained with anti-PTH antibody (ab213557, Abcam). The left lower panels in (**B**) and (**D**) show secondary antibody-only controls. Staining of kidney is non-specific (**D**). DAPI (cyan; **A** and **C**), PTH (green; **B** and **D**). Scale bars: 100 μm.

(**E**–**I**) Bulk RNA-seq data of grafted PTG cells. Differentially expressed genes analysis using DESeq2. log2(FC) means fold changes of grafted mESC-derived PTG cells gene counts against primary PTG cells (primary PTG cells, same samples as in Figure 3). Two weeks after renal subcapsular transplantation of mESC-derived PTG, the graft was removed and tdTomato-positive cells were sampled. (**J**) Volcano plot from log2(FC) and p-value.

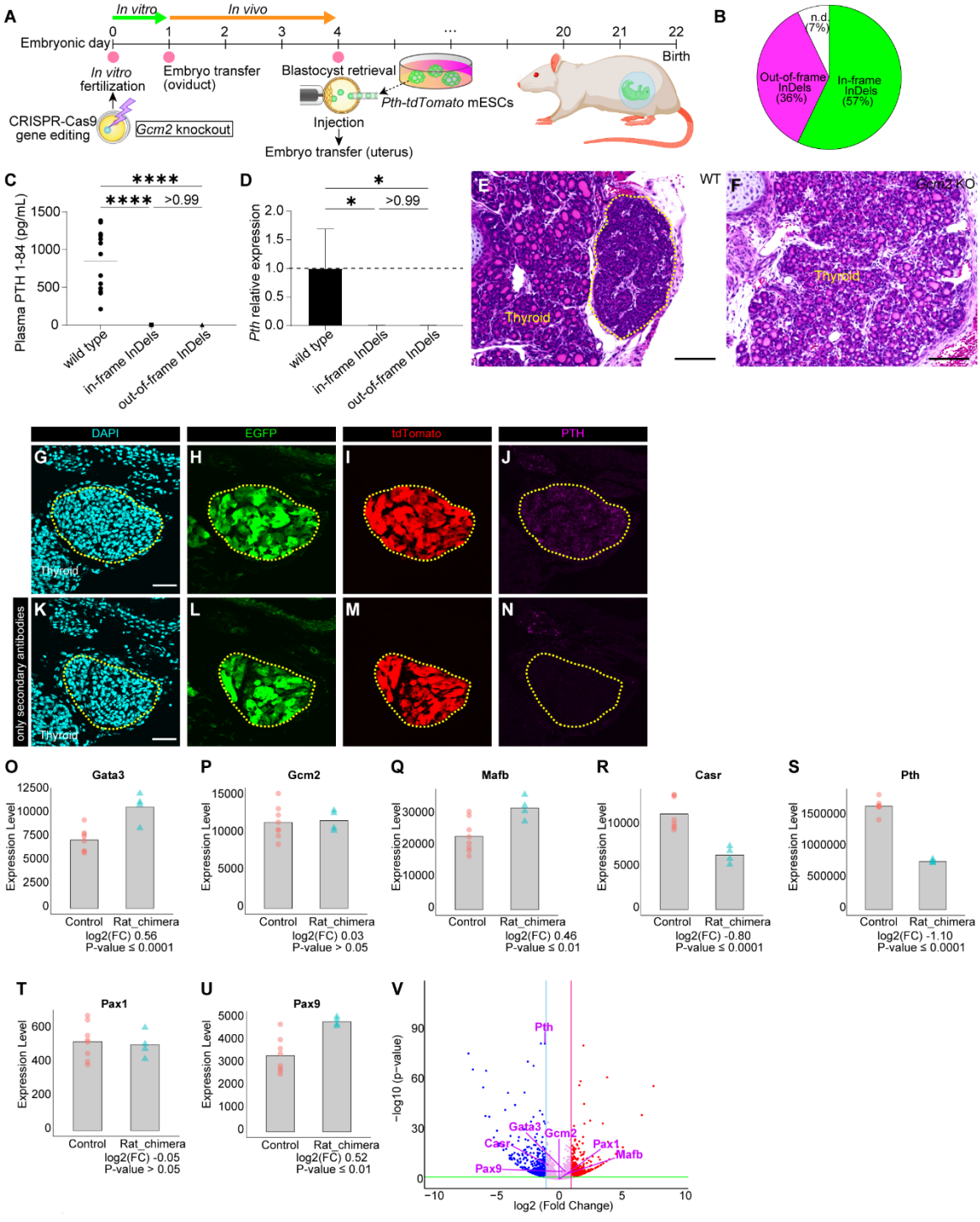

Supplementary Figure 6 (S6). Generation by interspecies BC of mESC-derived PTGs in *Gcm2* KO rat neonates.

(**A**) Strategy for single-step interspecies BC generation of mESC-derived PTGs in *Gcm2* KO rats. (**B**) Genotypes of *Gcm2* mutant newborns in rats. (**C**) Plasma PTH 1-84 levels in wild type Wistar rats and *Gcm2*$^{-/-}$ rats at the neonatal stage. Wild type, n=13. *Gcm2* mutants with in-frame InDels, n=11. *Gcm2*$^{-/-}$ rats with out-of-frame InDels, n=9. (**D**) *Pth* mRNA expression in wild type Wistar rats and *Gcm2*$^{-/-}$ rat neonates. Wild type, n=5. *Gcm2*$^{-/-}$ rats with in-frame InDels, n=5. *Gcm2*$^{-/-}$ rats with out-of-frame InDels, n=5. Graphed values, mean with s.d. (**E, F**) HE sections of wild type Wistar rats (**E**) and *Gcm2*$^{-/-}$ rats with out-of-frame deletion (**F**). Yellow dotted lines indicate PTGs. Scale bars: 100 μm. (**G**–**N**) Immunostaining of mESC-derived PTGs in the *Gcm2*$^{-/-}$ rat (**G**–**J**) and only secondary antibodies controls (**K**–**N**). Yellow dotted lines indicate PTGs. DAPI (cyan; **G, K**), GFP (green; **H, L**), tdTomato (red; **I**, **M**), PTH (magenta; **J**, **N**). Yellow dotted lines indicate PTGs. Scale bars: 100 μm. (**O**–**U**) Bulk RNA-seq data of mESC-derived PTGs in the *Gcm2*$^{-/-}$ rat. Differentially expressed genes analysis using DESeq2. log2(FC) means fold changes of gene counts of mESC-derived PTGs in *Gcm2*$^{-/-}$ rat ("Rat_chimera") against control (C57BL/6-*Pth*$^{tm1(P2A\text{-}tdTomato)/+}$ mouse). Same samples as in Figure 3. (**V**) Volcano plot from log2(FC) and p-value.
* $P \leq 0.05$, **** $P \leq 0.0001$, n.s., not significant using Kruskal-Wallis test with Dunn's multiple comparisons test (**C, D**).

Supplementary Tables

Table S1. Neonatal survival of *Gcm2* mutant pups on BDF1B6 background.

	Living fetuses	Genotypes of *Gcm2* mutants					
		Biallelic			Mosaic		
		Out-of-frame	In-frame	Both	Out-of-frame	In-frame	Both
At birth	22	8	8	5	1	0	0
Second postnatal day	1	1	0	0	0	0	0

Table S2. Count data, *Gfp*-high and *Gfp*-low expression, each cluster.

Cluster	Total counts	Counts, *Gfp*-high expression	Counts, *Gfp*-low expression	Percentage of *Gfp*-high expression
1	2604	2463	141	94.6
2	684	312	372	45.6
3	385	251	134	65.2
4	288	182	106	63.2
5	87	59	28	67.8
6	74	33	41	44.6
7	55	48	7	87.3
8	36	23	13	63.9
9	25	18	7	72.0

Table S3. *Gcm2* knock-out efficiency in Wistar rat offspring after zygote genome editing using CRISPR-Cas9.

Strain	Embryos transferred	Living fetuses	Genotypes of *Gcm2* mutants							
			Monoallelic		Biallelic			Mosaic		n.d.
				Out-of-frame	In-frame	Both	Out-of-frame	In-frame	Both	
Wistar	120	14	0	5	5	3	0	0	0	1

Those that could not be amplified by crude PCR with the mouse primer pairs were described as n.d.